

# Optical Coherence Tomography of Glass Reinforced Polymer Composites

Joy P. Dunkers, Richard S. Parnas, Carl G. Zimba  
Richard C. Peterson, and Kathleen M. Flynn  
Polymers Division  
National Institute of Standards and Technology  
Gaithersburg, MD 20899

James G. Fujimoto and Brett E. Bouma  
Department of Electrical Engineering and Computer Science  
and the Research Laboratory of Electronics  
Massachusetts Institute of Technology  
Cambridge, MA 02139

## Abstract

Optical coherence tomography (OCT) is a non-destructive and non-contact technique to image microstructure within scattering media. The application of OCT to highly scattering materials such as polymer composites is especially challenging. In this work, OCT is evaluated as a technique to image fiber tows and voids in two materials: an epoxy E-glass reinforced composite and a vinyl ester E-glass reinforced composite. Features detected using OCT are compared with optical microscopy. Fiber architecture and voids of glass reinforced polymer composites can be successfully imaged using OCT. The quality of the OCT image is strongly affected by the refractive index mismatch between the fibers and reinforcement. The largest sources of noise in the images arise from fiber lens effects, interference from within the sample, and a very large reflection at the surface.

Keywords: Optical coherence tomography, non-destructive evaluation, polymer composites.

Title abbreviation: OCT of Polymer Composites.

## Introduction

Non destructive evaluation (NDE) is an important topic in polymer composites because of the need to verify material specifications such as residual porosity, fiber architecture and structural integrity. In this work, optical coherence tomography (OCT) has been used to image composite microstructure. OCT has been used extensively to image the human retina<sup>1</sup>, skin and blood vessels<sup>2</sup>, and the operating circulatory system of small live animals<sup>3</sup> with excellent clarity. In this work, the sensitivity limits of this technique are being tested since it is used here for the first time to image very highly scattering materials: polymer composites.

Optical coherence tomography is a non-invasive, non-contact optical imaging technique that allows the visualization of microstructure within scattering media. OCT uses light in a manner analogous to the way ultrasound imaging uses sound and, while typically affording shallower penetration depth, provides significantly higher resolution (5-30  $\mu\text{m}$ ). OCT is based on low-coherence ranging: the optical distance to individual back-scattering sites within the sample is determined using an interferometer and a dispersive source. Multiple through thickness back-reflectance scans are registered while transversely scanning either the sample or the probing beam and are combined to form a cross-sectional image.

To perform OCT imaging, broad-spectrum laser light (20 - 200 nm bandwidth) is transmitted using a single mode fiber and coupled into a 50/50 fiber optic splitter that illuminates the sample and a linearly translating, constant velocity reference mirror. The fiber optic splitter, fixed sample and constant velocity reference mirror can be thought of as a Michelson interferometer. Light back-reflected from each interferometer arm is recombined at the fiber optic splitter. Interference fringes are registered at the detector only when the optical path length of the reference arm matches that of the sample arm to within the coherence length of the light source. The axial resolution with which this ranging can be performed is therefore determined by the coherence length or inverse

spectral width of the source. Therefore, the axial resolution can be as low as 5  $\mu\text{m}$ . Low coherence sources such as mode-locked solid-state pumped lasers or superluminescent diodes are used. Transverse resolution in OCT is determined by the focal spot size of the probing beam, which is usually 10-30  $\mu\text{m}$ . Higher numerical aperture optics provide superior transverse resolution, but at the expense of a diminished depth-of-field.

The full potential of OCT in the field of polymer matrix composites has yet to be assessed since more imaging should be performed on a larger variety of composites. However, a summary of established NDE techniques is presented below and provides some comparison with OCT. Ultrasound imaging is primarily used to observe defects with a resolution of hundreds of microns, works best with planar samples, and is used in through transmission or back scattering modes<sup>4</sup>. Unlike OCT, measurements are complicated by the requirement of a coupling medium between the transducer and composite<sup>4</sup>. Like OCT, ultrasound suffers from a degradation of feature contrast by shadowing of strongly scattering features from above. However, ultrasound can successfully image voids and damage in carbon fiber reinforced composites. It is anticipated that imaging of carbon fiber reinforced composites with OCT will be difficult because of the light absorption by the carbon fiber.

X-ray based techniques are used extensively to evaluate damage and, like ultrasound, have been applied less frequently to the examination of voids and tow placement. Composite damage has been studied with x-ray radiography<sup>5,6</sup>. All x-ray techniques rely on the contrast generated by the variation of the attenuation of the x-ray beam to differentiate heterogeneity from undisturbed material. Unlike ultrasound, this technique is non-contact. However, the best resolution requires the use a dye tracer to provide contrast between the damage zones and the rest of the composite. Also, superposition of features can confound interpretation with this conventional film radiography. A more recent technique, x-ray computed tomography (CT) relies on the measurement of transmitted radiation from many angles to reconstruct an image of the

composite<sup>7</sup>. X-ray CT can be used to detect various heterogeneities such as resin/fiber distribution, anisotropic fiber structure, voiding and porosity, as well as damage events. However, there are some drawbacks. X-ray CT is not amenable to flat composites or composites that have a large length-to-width ratio. The x-ray transmission is limited by the density, size and atomic number of material and x-ray source available. The damage must have a separation to be detected. Perhaps the biggest drawback is the spatial resolution, which is typically 500  $\mu\text{m}$ . With specialized sources and detectors, the spatial resolution can approach a few tens of microns with objects tens of millimeters in maximum dimensions at enormous cost<sup>7</sup>.

Nuclear magnetic resonance (NMR) imaging has been applied to composites with some success<sup>8</sup>, but has one major drawback. Imaging of glassy polymers such as epoxy is difficult because of the long spin-lattice relaxation ( $T_1$ ) that leads to line broadening and very short spin-spin relaxation ( $T_2$ ) that cannot be detected with current electronics. Thus, samples are usually imbibed with a liquid, and it is the relaxations of the liquid that are monitored. The spatial resolution is comparable to OCT, reportedly down to 10  $\mu\text{m}$ <sup>9</sup>. In addition, carbon fiber composites can be imaged in the majority of cases, except where the plane of the laminate sheets is perpendicular to the radio-frequency (RF) field since the conductive sheets screen the RF field within the coil<sup>10</sup>. But as with ultrasound, voids and other defects are usually imaged and not tow microstructure.

The objective in this first work is to identify the advantages and drawbacks of using OCT to image glass reinforced composites, define the material and acquisition conditions that provide the optimum images, and interpret the images. The ability of OCT to detect tow microstructure and voids is also evaluated. Future work will focus on imaging cracks, delaminations and damage zones, and using the images to compute preform permeability and mechanical properties.

## Experimental

### Instrumentation

The imaging system used in this study is schematically shown in Figure 1 and utilizes a 25 femtosecond mode-locked, chromium:forsterite solid-state laser as the optical source. The broad optical spectrum of this laser, centered at 1.3  $\mu\text{m}$ , and its high brightness make it an ideal source for OCT imaging. The laser light is coupled into a single-mode fiber-optic Michelson interferometer and delivered to both the reference mirror and the sample. The typical power applied to the sample is 3-4 mW. The reference mirror is mounted on a linearly translating galvanometer, which is driven with a triangular voltage waveform. The 260 mm/s velocity of this mirror results in a fringe modulation frequency of 400 kHz. Transverse scanning was performed using a computer controlled motorized stage to translate the sample.

The detection system was designed to use two photodiodes for dual-balanced detection so that amplitude noise from the laser source can be rejected. The interferometric signal was electronically filtered with a bandpass centered on the fringe or heterodyne frequency. The filtered fringe waveform is then demodulated, digitized and stored on a computer. The high dynamic range of this system allows back-reflections as weak as femtowatts of power to be detected. Images are displayed by mapping the logarithm of the signal strength to a gray-scale look-up table. The acquisition time for each image was approximately 1 minute.

The axial measurement range is determined by the distance the reference mirror moves (4.5 mm) normalized by the refractive index ( $n$ ) of the sample:  $4.5 \text{ mm}/n$ . The probe beam is focused to a 30  $\mu\text{m}$  diameter spot at a depth of approximately 750  $\mu\text{m}$  to 1000  $\mu\text{m}$  below the surface of the sample for the low resolution samples. The probe beam is focused to a 14  $\mu\text{m}$  diameter spot at a depth of approximately 200  $\mu\text{m}$  into the sample for the high resolution samples. The depth of field is  $(n)(1.0 \text{ mm})$  for low

resolution samples and  $n(0.25 \text{ mm})$  for high resolution samples, where  $n$  is the average refractive index for the composite.

The OCT images were taken for both the epoxy and vinyl ester resin composites with the fibers oriented perpendicular to the laser as shown in Figure 2. For any position along the  $x$  axis, reflections that represent heterogeneities are collected as a function of  $y$ . The sample is then moved with a motorized stage to image a new  $x,y$  slice of the composite, and this process is repeated for various positions along the fiber, or  $z$  axis. The transverse resolution along the  $x$  axis is estimated to be  $40 \mu\text{m}$  for the low resolution images and  $20 \mu\text{m}$  for the high resolution images. The transverse resolution is governed by spot size and scan rate, and there is an inverse relationship between transverse resolution and sampling depth. The axial resolution along the  $y$  axis is  $20 \mu\text{m}$  for the low resolution samples and  $10 \mu\text{m}$  for the high resolution samples. All images contain  $300 \times 300$  pixels and took about 1 minute to acquire. All samples were tilted  $4^\circ$  to avoid collection of the laser reflection from the top surface.

### Materials<sup>11</sup>

Two epoxy resin composites were molded with two amines having different relative concentrations. Both epoxy resin systems consisted of a diglycidyl ether of bisphenol A (DGEBA) monomer (Tactix123, Dow Chemical Company, Midland, MI) and two amines. Aromatic methylene dianiline (MDA) and aliphatic poly(propylene glycol)bis(2-aminopropyl ether) (JeffamineD400) ( $M_n \sim 400$ ) were purchased and used as received from Aldrich (Minneapolis, MN). The oxirane/ amine stoichiometry was 2 mol oxirane/1 mol amine. The amine composition that consisted of 0.75 mol MDA and 0.25 mol D400 was designated as the high refractive index or high index resin. The amine composition that consisted of 0.07 mol MDA and 0.93 mol D400 was designated as the low refractive index or low index resin. The refractive index of the low index postcured resin is 1.552, of the high index postcured resin is 1.614, and of the fibers is 1.554 as

measured by white light and index matching fluids. The refractive index of the epoxy composites is calculated by the rule of mixtures for the resin and the fiber volumes:  $V_{resin}=0.45$ ,  $V_{fiber}=0.55$ ,  $(n_{resin})(V_{resin}) + (n_{fiber})(V_{fiber}) = n_{composite} = 1.553$ . The axial length or depth of field is:  $4.5 \text{ mm}/1.55=2.9 \text{ mm}$  for each low index, low resolution image. The axial length is:  $3.0 \text{ mm}/1.58=1.9 \text{ mm}$  for each high index, low resolution image. The high index, high resolution images are scaled in a similar manner:  $1.1/1.58=0.70 \text{ mm}$ .

For the curing experiments, the MDA was melted (mp 89-90 °C). The room temperature DGEBA monomer was added to the melted MDA, and the mixture was stirred until homogeneous. After cooling the mixture to about 50 °C, the D400 component was added and stirred until homogeneous. The mixture was then poured into the room temperature resin transfer molding (RTM) pressure pot. The resin was injected into a flat plate mold that contained 7 layers of Knytex weft unidirectional D155 fabric (Owens Corning, Toledo, OH). The details of the resin transfer molding system have been previously described<sup>12</sup>. The epoxy was degassed at -90 kPa for 10 min prior to mold filling, and the mold wall temperature was monitored.

The vinyl ester resin composites were prepared as follows<sup>13</sup>: Rovings of E-glass fibers were unspooled from the interior of a spool supplied from Vetrotex Certaineed Corporation (Wichita Falls, TX). The cross-section of the rovings was elliptical with a major axis of 4.55 mm and a minor axis of 0.22 mm. The rovings had a 20/1 aspect ratio and consisted of 1600 fibers, 22.45 μm in diameter. The rovings were drawn through a glass tube mold 6.86 mm inner diameter which had previously been cleaned with acetone and dried in an oven at 100 °C.

The resin system consisted of a vinyl ester resin, Derakane 411-C50, from Dow Corning (Midland, MI) mixed with 1% by weight of an elevated temperature curing agent, 2,5-Dimethyl-2,5-di(2-ethylhexanoyl peroxy)hexane, USP-245, from Witco Corporation (Richmond, CA). The chilled curing agent was mixed with the resin at 23 °C. The mixture was then allowed to stand for 30 min and was followed by additional

stirring. The resin was then poured into the RTM apparatus. The mixture has a viscosity of 125 cp at 23 °C. The refractive index of the resin mixture:  $n_D^{25^\circ\text{C}} = 1.562$

The glass tube was connected to a RTM apparatus and the vinyl ester resin mixture was introduced into the mold by applying compressed nitrogen pressure on the resin reservoir. The voids were controlled by the application of low or high amounts of nitrogen pressure. The flow was allowed to continue at constant pressure until the desired level of saturation was achieved. The mold was then sealed, disconnected from the RTM set-up, placed into an oven preheated to 100 °C, and cured for 30 min followed by a post-cure of 150 °C for 2 hrs. The composite was removed from the glass tube and sectioned. The void volume of the low void sample was 6% while the high void sample was 45%. The fiber volume fraction was 51.4% for the high void sample and 61.7% for the low void sample. The refractive index of the resin was 1.572 and of the glass fiber was 1.550 from white light and index matching fluids. The voids were taken into account in the rule of mixtures calculation of refractive index. The refractive index of the low void sample was 1.55 and that of the high void sample was 1.46.

The vinyl ester resin composites were prepared for optical microscopy as follows: A 100  $\mu\text{m}$  gold transmission electron microscopy grid was shadowed onto the sample. The samples were polished to the position along the fiber axis that corresponded with the OCT image. The error in position between the OCT image and optical microscopy was estimated to be 30  $\mu\text{m}$ . However, this small positional error is of little consequence since the features in the composites extended over hundreds of microns.

## Results and Discussion

The composite samples of initial interest for OCT were composed of 7 layers of unidirectional Knytex fabric with the low refractive index epoxy resin. Figure 3 shows an OCT image of the entire cross-section of the composite. The image is 6 mm wide and 3.7 mm deep. Each tow is typically 1 mm wide and 550  $\mu\text{m}$  thick. This image is a composite

of two images taken from the top and bottom of the sample at the same position along the fiber axis, and the bottom image quality is slightly degraded compared to the top image. The dark ellipses indicated by an arrow are the threads that are stitched to hold each layer of the fabric together.

The resin, fibers, and voids are differentiated by the amount of light reflected back from an interface between two materials of different refractive indices. By definition, the sum of the reflectance (R), transmittance (T), and absorptance ( $\alpha$ ) is equal to unity:  $T + R + \alpha = 1$ . In this system, we assume that the absorptance of the laser is negligible. Thus,  $T + R = 1$ . In other words, the more the light is reflected, the lower the penetration of the beam into the sample. The intensity of light reflected back increases with increasing refractive index mismatch between the two materials and as the source wavelength decreases. The light regions outside of the tows are identified as resin rich areas and the medium gray regions are the fiber tows. The black spots within the fiber tows could be voids from incomplete wetting of the fiber tows and consequent air entrapment. However, care must be taken when interpreting these images for the following reasons.

The contrast between voids, fiber tows, and resin decreases as a function of the depth within the sample (y axis) because the reflected signal is getting weaker as the light penetrates the sample. For this particular figure, since it is a composite of top and bottom images, the noise increases as you move towards the center of the sample thickness. The intensity of the light reaching a particular depth for any position across the sample is affected by how strongly features directly above that position reflect or randomly scatter the light, which for this sample, while somewhat regular, were not easily predicted. Therefore, for any particular depth within the sample, a gray-scale value of a pixel or group of pixels cannot be assigned to a particular feature upon first inspection. For example, a light area within a tow could result from a resin rich region, the destructive interference of a group of fibers, or shadowing from a strongly reflecting feature from above. In addition to lens and interference effects in the sample, another source of noise

is the gray vertical lines that project from the black reflection that is the air/composite interface. These lines are a result of detector saturation at that strongly reflecting interface. In fact, the noise from the instrumentation is far below the level of noise generated from the sample itself. For a resolution of 15  $\mu\text{m}$ , dynamic range using the solid state laser source is -115 dB.<sup>14</sup> From the above discussion, the best way to differentiate real features from artifacts is to evaluate a number of slices.

The binary image in Figure 4 is generated from Figure 3 to better display the tow shape and placement. The binary image was created using NIH Image<sup>15</sup> by first applying the one dimensional vertical background subtraction to remove the vertical lines generated by the detector saturation. Then, density slicing was applied so that the fiber tows were as filled as possible but not altered in size and shape. Lastly, the density sliced data was made binary. This figure shows that most of the layers of tows lie in the spaces of the layer above and below. The bottom two layers are exceptions. These fiber tows lie almost directly on top of one another. Information about the relative placement of fabric layers could be used in the calculation of mechanical properties thereby eliminating the need to make those assumptions and improving the accuracy of the calculation. Also, a three dimensional reconstruction and reslicing could reveal information about tow displacement during injection, another important piece of information for mechanical property calculations.

Another important influence on the quality of OCT images is the refractive index mismatch between the resin and the fibers. Figure 5a shows an image using the high index resin. However, barely two layers of the composite can be differentiated and contrast is rapidly lost in the axial direction. With the low index resin in Figure 5b, 4-5 layers can be seen clearly with good contrast within the tows.

Figure 6 contains high resolution images of the fiber tow that appears the second from the right in Figure 5a. The image dimensions are 2 mm wide and 1.1 mm/n or 0.71 mm deep, and the black irregular areas are nominally 170  $\mu\text{m}$  wide and 180  $\mu\text{m}$  deep.

The axial resolution is 10  $\mu\text{m}$  and the transverse resolution is 20  $\mu\text{m}$ . High resolution images of structure deeper into the sample can be acquired by adjusting the position of the focal point into the sample. The large, dark areas in each image are thought to be voids that extend at least 400  $\mu\text{m}$  through the sample. Samples were obtained with known volume average porosity to better evaluate how voids appear in the images.

Figure 7 displays the OCT cross-sectional images of the low (a) and high (b) void samples. These images are uncorrected in the axial direction. Because of the very large aspect ratio of the fiber tows, the composite samples can be considered to be continuous fibers. In Figure 7a, the small gray and black speckles near the top of the image are the individual fibers. As discussed before, the contrast fades as a function of depth in the images, so fewer of the individual fibers can be discerned. In Figure 7b, some individual fibers can be identified. More importantly, there are larger black features that can be correlated with the existence of voids, as shown in the next figure.

Figure 8a is the re-scaled Figure 7b and compares the OCT image of the high void content composite with the corresponding optical micrograph, 8b. The OCT image was collected at 260  $\mu\text{m}$  in the z direction while the optical micrograph was taken at 270  $\mu\text{m}$ . From multiple OCT images, these voids extend from at least 180 $\mu\text{m}$  to 360 $\mu\text{m}$ . The dimensions of Figure 8a are 5.1 mm wide and 1.9 mm deep, and the dimensions of Figure 8b are 5.1 mm wide and 1.8 mm deep. The voids observed in the micrograph image, 8b, can be seen in the OCT image, 8a, but the delineation of the void boundaries are not as pronounced. The dotted lines show the correspondence of representative features in the OCT and the optical microscopy images. The resin rich areas in Figure 8b are not detected in the OCT image.

Figure 9a displays an OCT image of the low void sample and the corresponding optical micrograph in Figure 9b. The dimensions of Figure 9a are 6.0 mm wide and 1.9 mm deep. Although some correspondence can be made at shallow penetration depths, it is difficult to identify the resin rich areas in 9a that are so prominent in the 9b. The

dimensions of Figure 9b are 6.2 mm wide and 1.7 mm deep. Figure 9b is 170  $\mu\text{m}$  along the z axis. Multiple OCT images are essentially identical from 180  $\mu\text{m}$  to 2180  $\mu\text{m}$  along the z axis. The OCT image is featureless for a couple of reasons. The first is the previously mentioned attenuation as a function of depth. The second is the fact that since boundaries are blurred in this technique, the detection of small features that do not have large refractive index differences like embedded voids, becomes difficult. Despite its caveats, OCT is a technique that has the potential to extract a great deal of information from composites in a non-destructive manner.

## Conclusions

Glass reinforced polymer composites can be successfully imaged using OCT. However, the quality of the OCT image is strongly affected by the refractive index mismatch between the fibers and reinforcement. In this work, OCT was used to investigate the microstructure nominally to a depth of 2 mm as collected or 4 mm when both top and bottom images were reconstructed. Low resolution images have a 40  $\mu\text{m}$  transverse and 20  $\mu\text{m}$  axial resolution while high resolution images have a 20  $\mu\text{m}$  transverse and 10  $\mu\text{m}$  lateral resolution. The largest source of noise in the images arises from fiber lens effects and interference from within the sample and a very large reflection at the surface. Lastly, images must be interpreted carefully because of attenuation of contrast through sample thickness. Inspection of multiple slices or a three dimensional reconstruction are the best methods for identifying real features.

## Acknowledgements

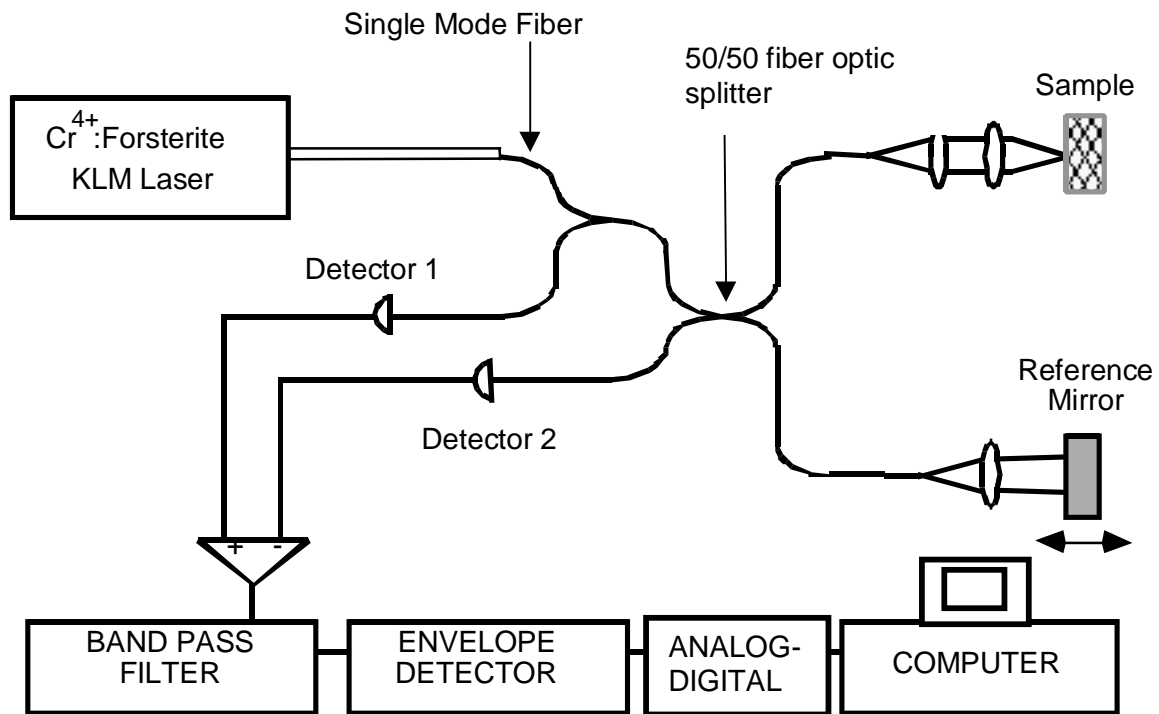
The authors would like to acknowledge Dr. Catheryn Jackson of NIST for her help with optical microscopy.

## References

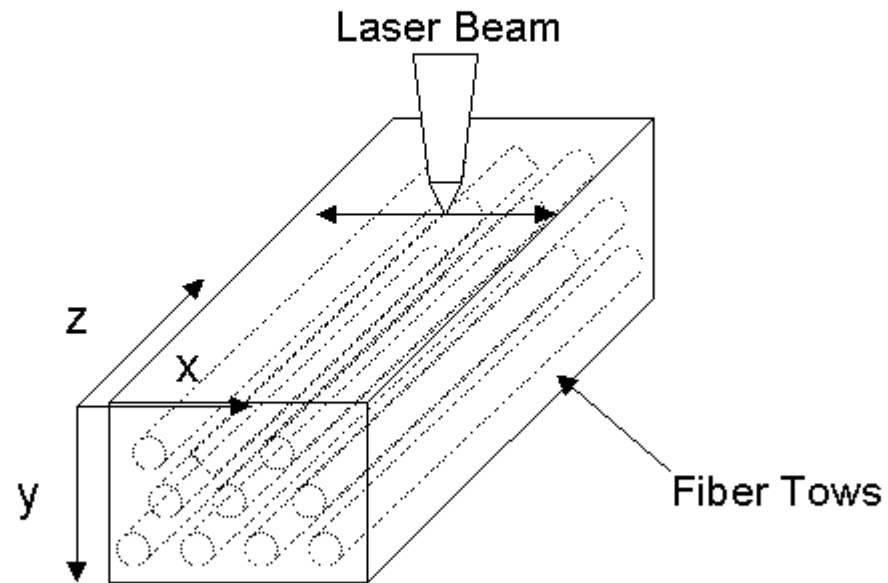
1. Hee, M., Izatt, J., Swanson, E., Huang, D., Schuman, J., Lin, C., Puliafito, C. and Fujimoto, J. *Archives of Ophthalmology*, 1995, **113**, 325.
2. Barton, J., Milner, T., Pfefer, T., Nelson, J. and Welch, A. *J. of Biomed. Opt.*, 1997, **2(2)**, 226.
3. Boppart, S., Brezinski, M., Bouma, B., Tearney G. and Fujimoto, J. *Developmental Biology*, 1996, **177**, 54.
4. Wooh, S. and Daniel, I. *Materials Evaluation*, 1994, **48(5)**, 1199.
5. Highsmith, A. and Keshav, S. *J. Comp. Tech. & Res.*, 1997, **19(1)**, 10.
6. Kortschot M. and Zhang, C. *Comp. Sci. & Tech.*, 1995, **53(2)**, 175.
7. Bossi, R. and Georgeson, G. *Materials Evaluation*, 1995, **53(10)**, 1198.
8. Hoh, K.-P., Ishida, H. and Koenig, J. *Polymer Composites*, 1990, **11(3)**, 192.
9. Blumich, B. *Adv. Mater.*, 1991, **3(5)**, 237.
10. Jezzard, P., Wiggins, C., Carpenter, T., Hall, L., Barnes, J., Jackson, P. and Clayden, N. *J. Mat Sci.*, 1992, **27(23)**, 6365.
11. Identification of a commercial product is made only to facilitate experimental reproducibility and to adequately describe experimental procedure. In no case does it imply endorsement by NIST or imply that it is necessarily the best product for the experimental procedure.
12. Dunkers, J., Flynn, K. and Parnas, R. *Composites, Pt. A.*, 1996, **28(2)**, 163.
13. Peterson, R. Ph.D. Dissertation, University of Michigan, Ann Arbor, MI, 1996.
14. Bouma, B., Tearney, G., Bilinsky, I., Golubovic, B. and Fujimoto, J. *Opt. Lett.*, 1996, **21(22)**, 1839.
15. The public domain NIH Image program was developed at the U.S. National Institutes of Health and is available on the Internet at <http://rsb.info.nih.gov/nih-image/>.

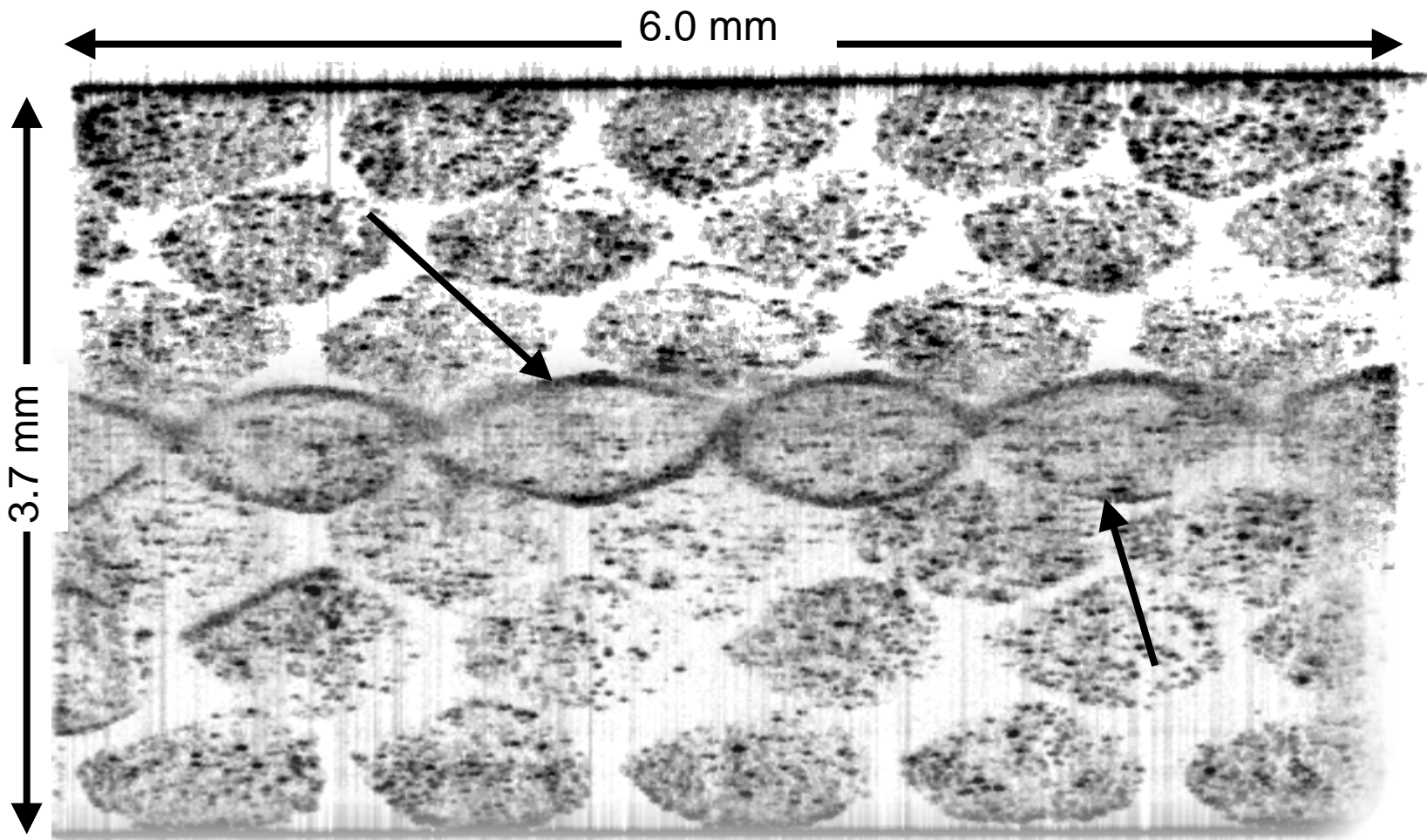
## Figure Captions

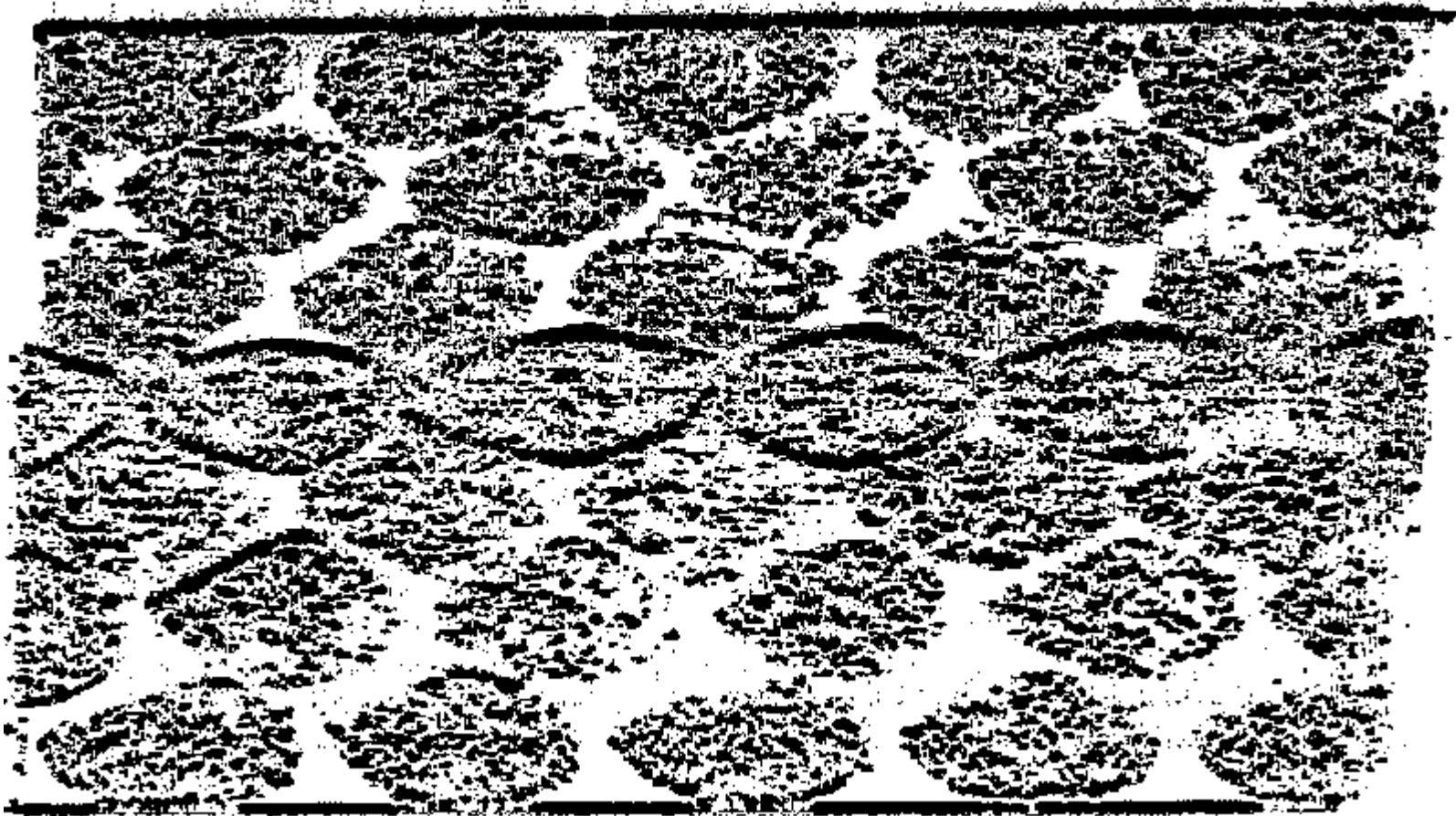
- Figure 1: Schematic representation of the solid state laser and OCT system layout.
- Figure 2: Schematic showing the laser orientation and sampling directions with respect to the composite.
- Figure 3: As collected OCT image of unidirectional E-glass fibers in epoxy resin.
- Figure 4: Figure 3 as a binary image.
- Figure 5: Low resolution images of high index (A.) and low index (B.) composites.
- Figure 6: High resolution images of the high index resin at 0  $\mu\text{m}$  (A.), 100  $\mu\text{m}$  (B.), 200  $\mu\text{m}$  (C.), 300  $\mu\text{m}$  (D.), and 400  $\mu\text{m}$  (E.) from sample end.
- Figure 7: Images of vinyl ester resin/E-glass composites with low (A.) and high (B.) void content.
- Figure 8: Comparison of OCT image (A.) and optical micrograph (B.) for high void vinyl ester resin/E-glass sample.
- Figure 9: Comparison of OCT image (A.) and optical micrograph (B.) for low void vinyl ester resin/E-glass sample.



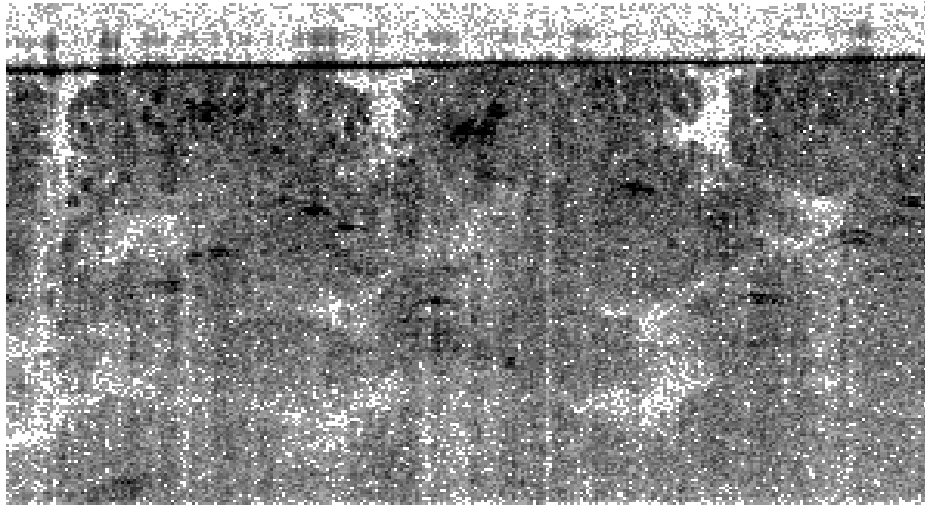
## Orientation of Composite with Laser Beam



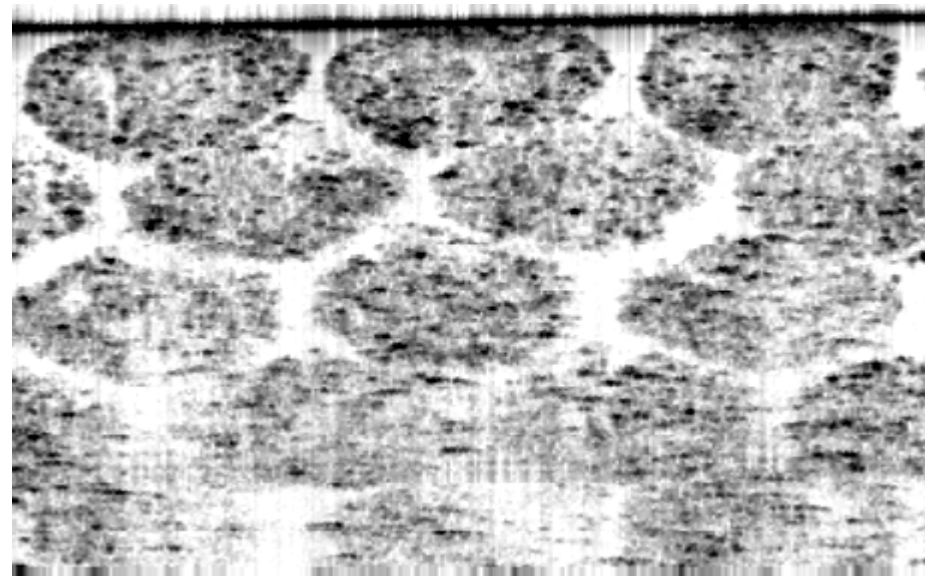


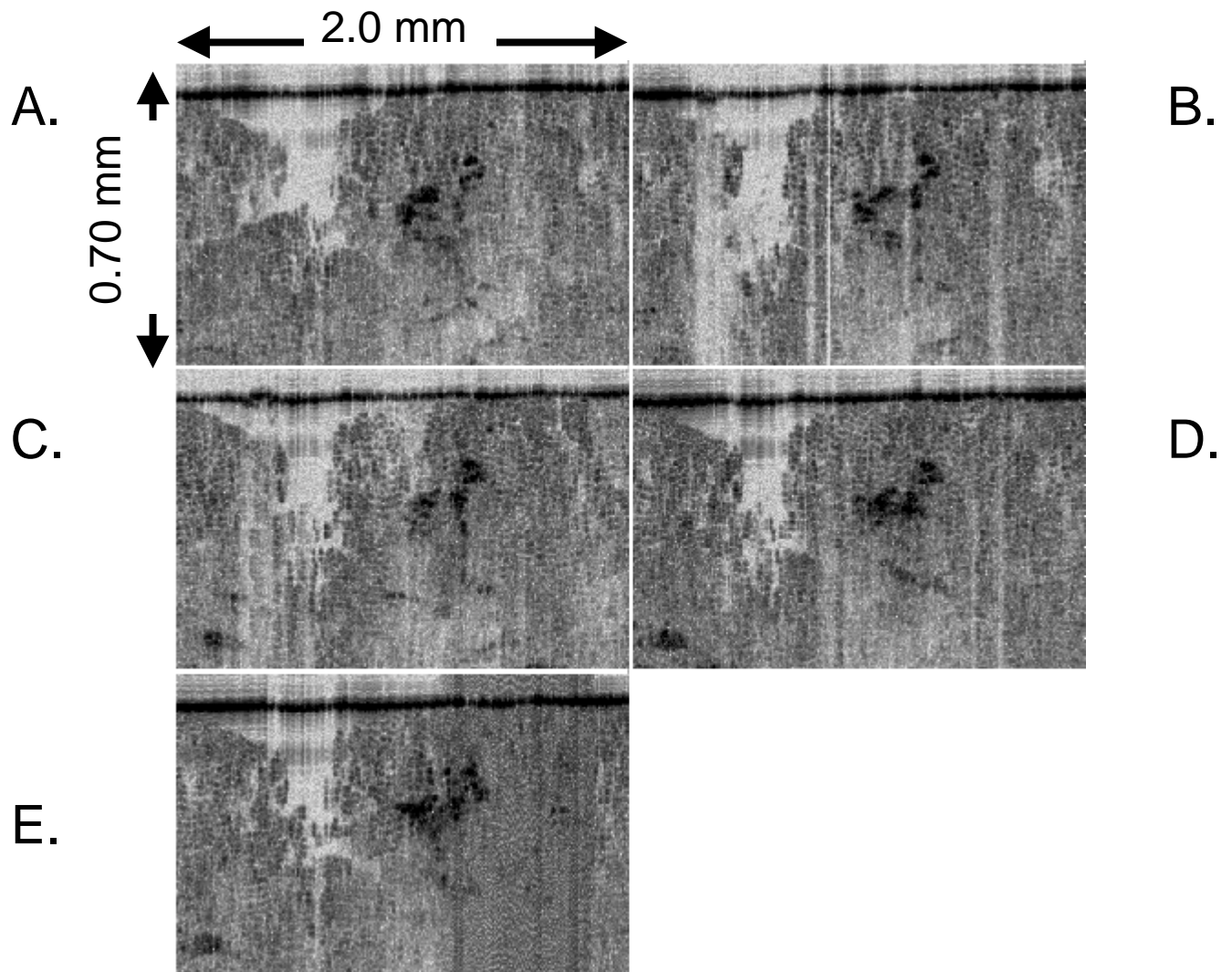


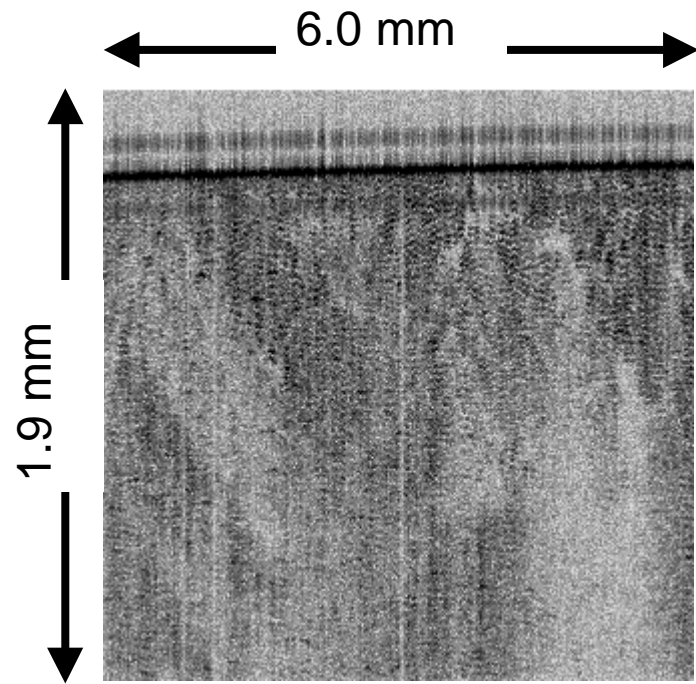
A.



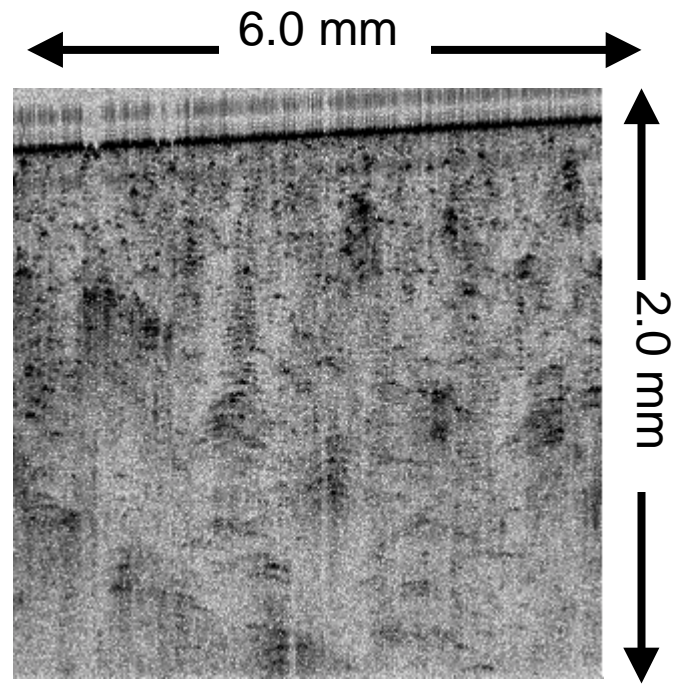
B.





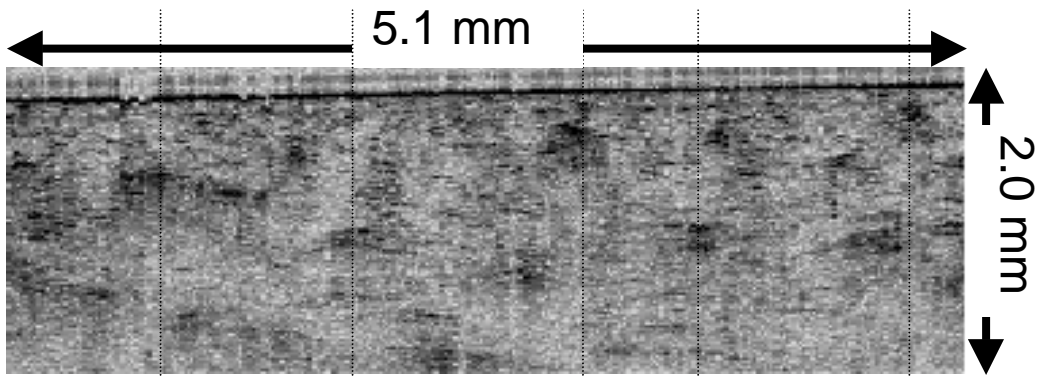


A.

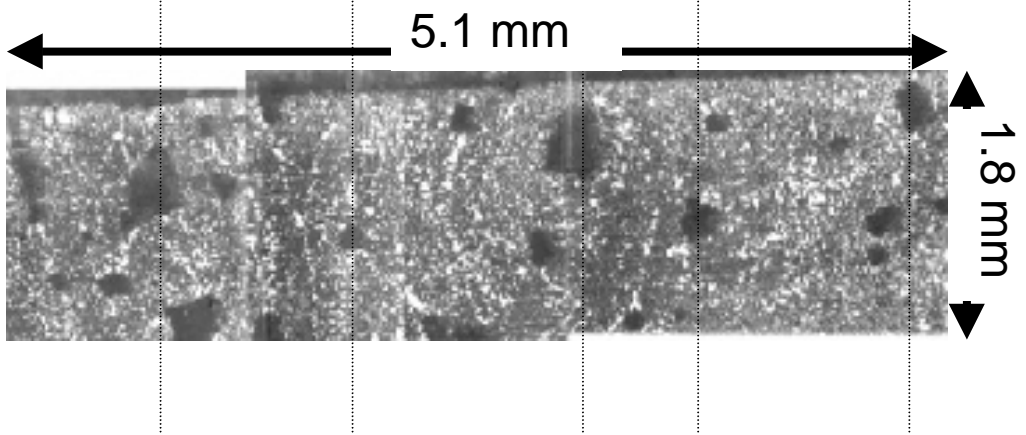


B.

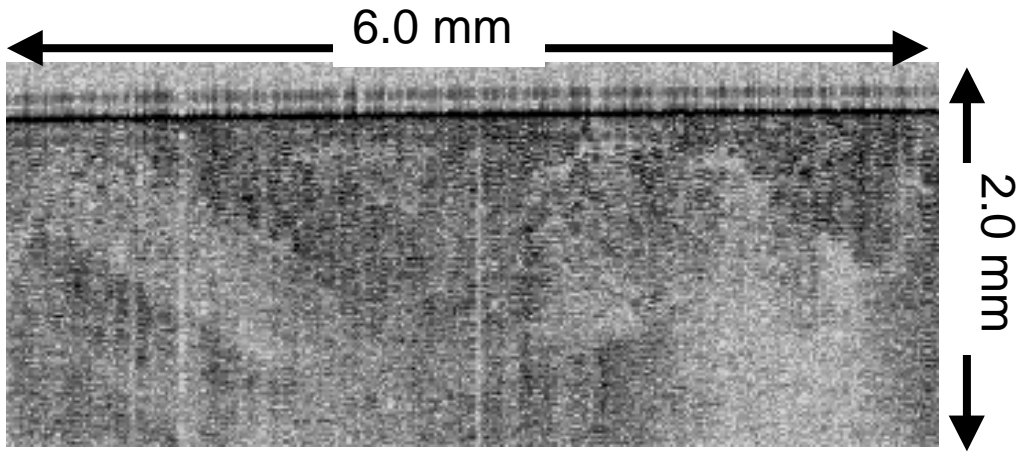
A.



B.



A.



B.

